JOURNAL OF MATERIALS SCIENCE 11 (1976) 273–282

Tensile strength and crack nucleation in boron fibres

JORGE VEGA BOGGIO, OLOF VINGSBO
Institute of Technology, Uppsala University, Uppsala, Sweden

Boron fibres of about 100 μm diameter have been tested to fracture in a micro-tensile testing machine. The fracture surfaces have been investigated using a scanning electron microscope and classified according to the fracture nucleation type. Comparison with the measured fracture stresses proved a significant correlation with the type of crack nucleation. Transverse cracks, nucleated at the edge of radial cracks along the fibre axis direction, are the most critical weakening feature. Also crack nucleation at the external fibre surface implies a low tensile strength, and is discussed in terms of a notch effect of the well-known nodular surface topography.

1. Introduction

Boron fibres (or filaments) are known to have very high strength and modulus of elasticity (of the order of 3×10^3 and 4×10^5 N mm^2 respectively) together with related properties, such as high hardness and melting point. Considering the low density of the material (2.6×10^3 kg m^{-3}), boron fibres constitute one of the most promising alternatives for fibre reinforcement, when light weight constructions are necessary. An increasing attention is paid to the relation between structure and mechanical properties, particularly fracture strength.

The present study is a contribution to the identification of crack nucleation mechanisms and the correlation between tensile strength and crack nucleation.

1.1. Manufacturer and morphology

Amorphous boron fibres are manufactured by chemical vapour deposition, as suggested by Talley *et al.* [1] in 1959. Boron trichloride and hydrogen react on a tungsten wire, 10 to 12 μm diameter, electrically heated to about 1500 K. Deposited boron diffuses into the substrate, which recrystallizes and transforms to a core of a polycrystalline mixture of borides (WB, W_2B_5 and WB_4). An amorphous boron mantle grows radially in conical grains, which gives the external surface a characteristic nodular topography.

The reaction takes place in a chamber, to which the continuous fibre has access through conducting mercury seals. Multistage systems are in wide use, and each time the growing fibre passes a seal, it is quenched. A final diameter of 80 to 120 μm is usually chosen.

1.2. Residual stress

The unidirectional diffusion into the core causes an increase in core diameter during the mantle growth. This results in a compressive residual stress in the core, and a dilational stress in the surrounding mantle. The quenching, finally, implies a compressive residual stress in the outer part of the mantle.

1.3. Fracture

The fracture surfaces of boron fibres essentially resemble those of glass rods, and have been divided into three zones, according to appearance and crack propagation velocity [2, 3].

(i) The mirror zone is very smooth, marks the initiation of the crack and corresponds to low velocity.

(ii) The mist zone has a matt surface and corresponds to higher velocity.

(iii) The hackle zone, finally, displays surface steps and ridges, caused by the deviation from

a single propagation plane for the highest crack velocities.

Further, radial cracks have been observed, extending along the fibre, from the core to the transition region between dilational and compressive residual stresses in the mantle. It is not agreed upon whether these cracks are frequently present, as a result of the residual stresses, or occur only incidently, or are created by the very fracture events.

In addition, Layden [3] has reported another type of fracture ("type II"), with a very smooth surface all across the mantle, except for a "gull wing" pattern and a residual fracture.

1.4. Crack nucleation

Since the beginning of the investigation of boron fibres, interest has been devoted to the initiation of fracture. Generally, the crack nucleation is related to fibre imperfections, sometimes referred to as flaws. With some generalization, the main observations of crack nucleation sites, reported in the literature [3–7], can be summarized as follows.

(i) Surface flaws, such as accidental damage points or nodule boundaries.

(ii) Crystalline or abnormally protruding amorphous nodules.

(iii) Inclusions in the core-mantle interface or in the mantle, generally in the case of multistage fibres.

(iv) Voids near the core–mantle interface. These voids are thought to result from the undirectional flow of boron from the mantle into the core [8].

(v) Notches in the initial core surface. Voids have been observed at the bottom of deep and narrow notches, possibly a result of diffusion induced pinching-off of a notch neck [3].

(vi) The interior of the core. Crack nucleation has been observed without relation to any detectable imperfections.

1.5. Correlation with tensile strength

Wawner [8], Layden [3] and Line and Henderson [5] have found that it is possible to relate different types of fracture mechanisms to tensile strength, σ_f. The strongest fibres ($\sigma_f \sim 4 \times 10^3$ N mm^{-2}) are related to core fracture according to point (vi) above, while all types of defects successively weaken the fibre down to below 1.4×10^3 N mm^{-2} (surface flaws).

2. Material and experimental

2.1. Material

Three spools of continuous fibres, A_1, A_2 and B were laboratory produced in multistage processes under highly varied experimental conditions by two manufacturers, A_1 and A_2 by Societé Nationale des Poudres et Explosifs, Paris, France and B by Lumlampan AB, Stockholm, Sweden. The core diameters were about 18 μm (A) and 14 μm (B) and the outer diameters were about 105 μm (A) and 87 μm (B).

2.2 Tensile testing

100 tensile test specimens of 50 mm length were cut at random from each spool. Preliminary tests had shown a tendency towards explosive failure (cf. [3]). Therefore, half of the specimens were mounted between a sheet of paper and adhesive tape, covering the gauge length in order to retain the debris for fractographic studies. No difference was observed in the strength distribution between "coated" and "non-coated" samples. Further, because less than 20% of the non-coated samples showed the explosive type of fracture, it was possible to extend the fractographic studies to more than 90% of the total number of tested samples.

The fibres were tested in a Lorentzen & Wettres (ALWETRON) micro-tensile testing machine. The contact between the metallic grips and the fibre was improved by the use of emery paper. All fibres were tested with a gauge length of 25 mm and a strain–rate of 3×10^{-3} s^{-1}. Fibre diameters were determined individually by means of a Mikrokator.

2.3. Morphology studies

20 specimens of 100 mm length were cut at random from each spool and given an electrolytical coating of nickel. The resulting composite was polished, ion-etched and studied in transverse sections in a JEM 200 B scanning transmission electron microscope, operated at 200 kV.

Fractured fibres were mounted in a specially made, rotatable and tiltable holder for 6 SEM specimens. The specimens were washed successively in trichlorethylene, acetone and alcohol, gold–platinum coated and studied in a JSM-U3 scanning microscope, operated at 20 kV.

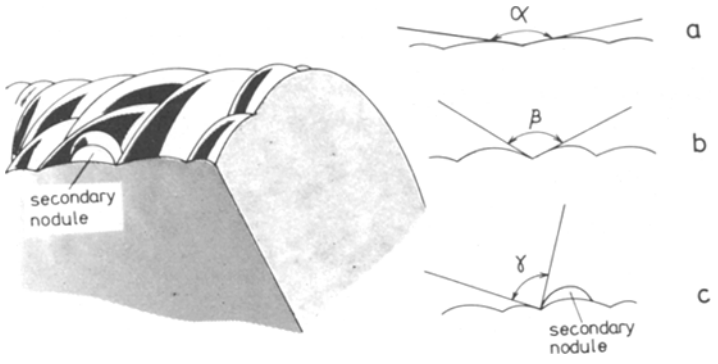

Figure 1 Schematic view of a longitudinal section of a fibre. (a) "Well oriented" nodular growth. The nodule boundary notch angle is α. (b) "Badly oriented" nodular growth. The nodule boundary notch angle is $\beta < \alpha$. (c) "Secondary" nodular growth. The nodule boundary notch angle is $\gamma < \alpha$.

3. Results and discussion

3.1. Classification of fracture types

In the present study, the fracture surfaces are classified according to the particular flaw, triggering failure. A common way to trace the fracture initiation site is to extrapolate the hackle marks back through the mist zone to a small area within the mirror zone. The following types of fracture are considered, and discussed in relation to previous findings.

3.1.1. Inclusions

Although the investigated fibres were manufactured in multistage processes, no inclusion initiated fracture of the type hitherto reported, was observed. This is a consequence of improved technical precautions as to cleanliness, and this type of fracture will not be further discussed.

3.1.2. Nodule boundaries, abnormal nodules

It is obvious that the nodule boundaries have a more or less pronounced notch effect, implying local stress concentrations in a fibre under external load. An important parameter, in this respect, is the notch angle, i.e. the angle between the nodule tangents at the bottom of a nodule boundary in a longitudinal plane according to Fig. 1. The more accute an angle, the higher is the stress concentration, and the more effective is the notch.

Often the quality of boron fibres is judged according to the appearance of the nodular surface structure. So called "well oriented" nodular growth [9] gives a rather smooth surface, with large notch angles (Fig. 1a), while "badly oriented" nodular growth gives a corn-cob surface with smaller notch angles (Fig. 1b) and consequently a lower nominal fracture stress. The phenomenon has also been referred to as abnormal nodular growth [3, 5], and ascribed

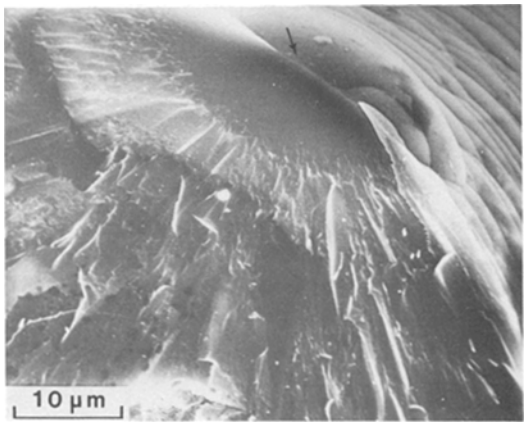

Figure 2 SEM micrographs of low angle (β) notch initiated fracture (fibre B, $\sigma_f = 27.8 \times 10^2\,N\,mm^{-2}$). Note that the initiation site coincides with the boundary of the abnormally grown nodule at the arrow.

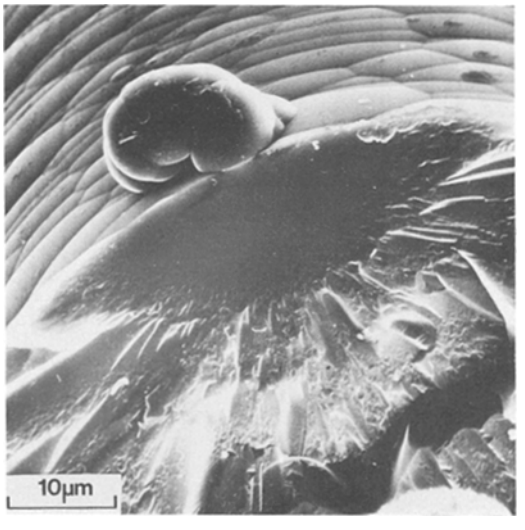

Figure 3 Fracture initiated at a secondary nodule (fibre B, $\sigma_f = 23.8 \times 10^2\,N\,mm^{-2}$). The hackle marks point to the crack nucleation site in a triple nodule boundary.

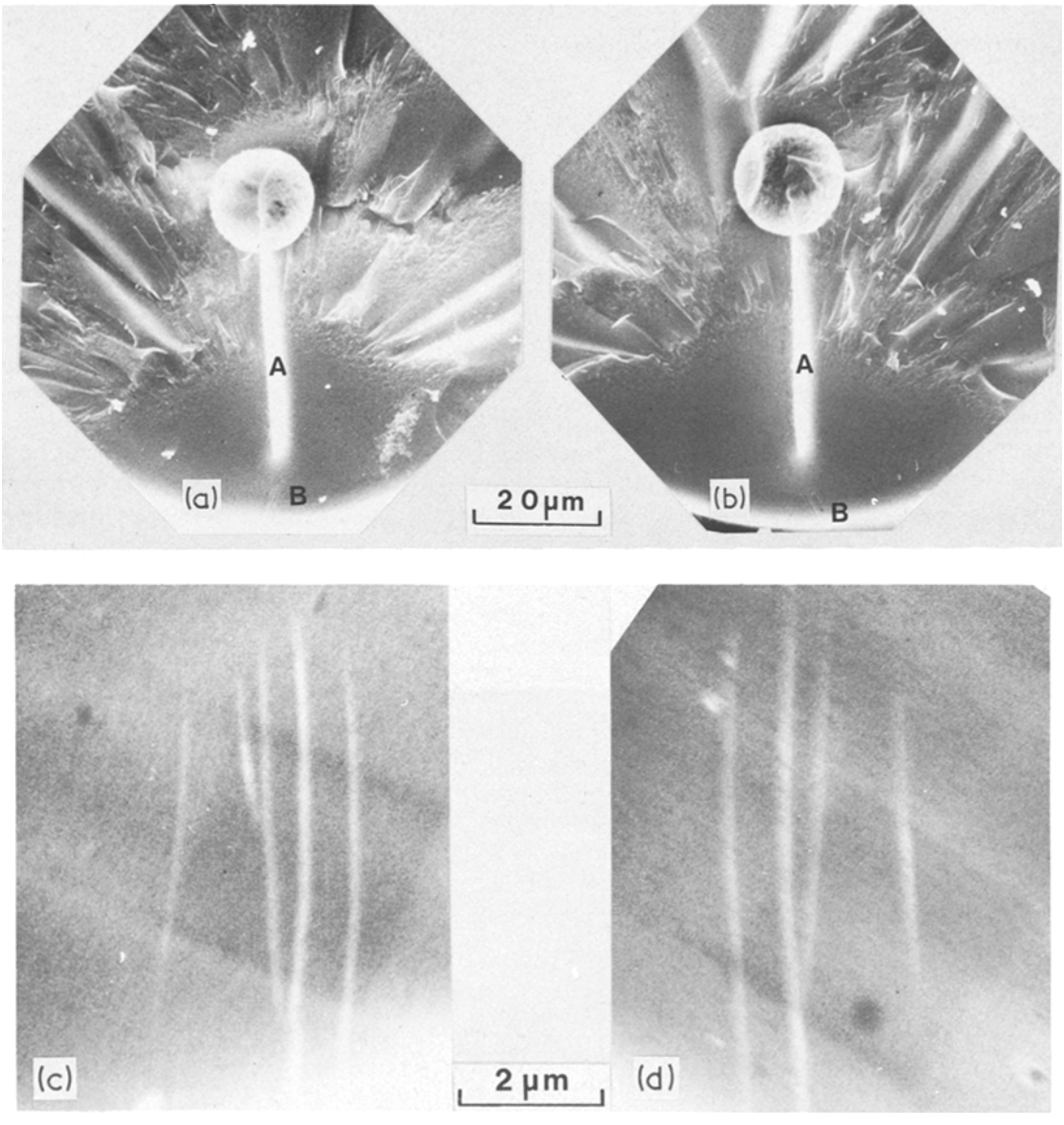

Figure 4 Two opposing fracture surfaces (fibre A_2, $\sigma_f = 12.5 \times 10^2 N\,mm^{-2}$) (a and b) Low magnification micrographs, showing hackle marks converging to the outer edge of a radial shear crack. (c and d) Small surface steps outside the nucleation site (at B in Fig. 4a and b).

the accentuated nodular growth around some inclusion. This type of nodule, however, cannot be expected in the present case (and were not observed) because of the clean process. There is, however, experimental evidence [9] that the nodular growth can also be controlled by reaction parameters, such as temperature.

Fig. 2 is a SEM image (emissive mode) showing an example of crack nucleation exactly at the bottom of a rather deep nodule boundary. Examples of this type of notch effect were numerous in fibres with badly oriented growth, but were never found in fibres with well oriented growth.

It is thus concluded that nodule boundaries are active as crack nucleating "surface flaws" if the corresponding notch angle is smaller than a critical value.

3.1.3. Nodule boundaries, secondary nodules

Carlsson [9] has found secondary nucleation of nodules for low final reaction temperatures. If secondary nucleation takes place immediately

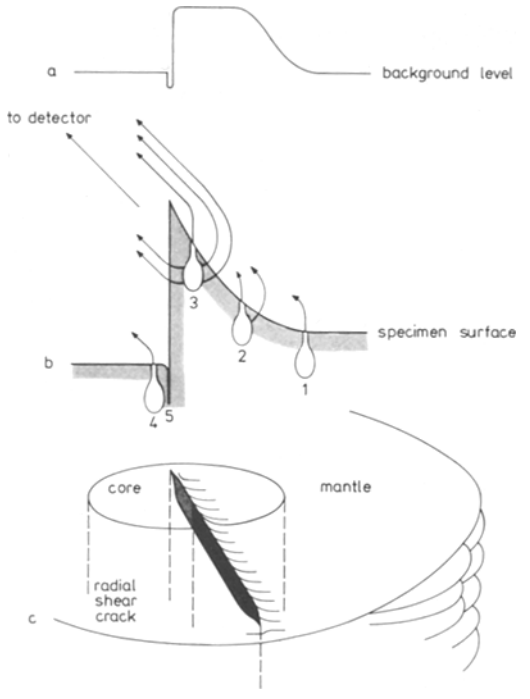

Figure 5 (a) Schematic intensity profile across the light band (A) in Fig. 4a and b. (b) Topography, giving the contrast of Fig. 5. When the incident electron beam hits the specimen at position 1, a low emitted intensity corresponds to the dark background. When the beam scans to the left, the emitting volume will come closer to the inclined exit surface (position 2), and the intensity will increase to a high constant level (position 3), corresponding to emission through both sides of the protruding tip. At the sharp edge there is an abrupt drop to a background level (position 4). Close inspection reveals a tiny dark contrast at the edge, interpreted as a fissure (position 5). (c) Perspective drawing of the fracture surface topography according to Fig. 4a and b and Fig. 5b.

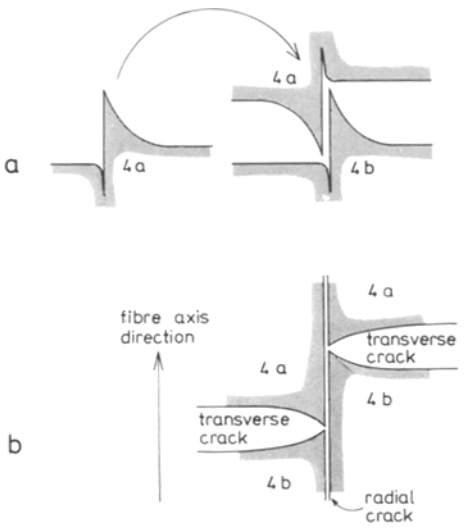

Figure 6 (a) The left–right similarity of the topography of Fig. 4a and b shows how the two fracture surfaces fit together along a step. (b) The surface step can be explained as a radial shear crack, separating two parts of a transverse crack on two different propagation planes.

before the wire leaves the final mercury seal, small wart-like nodules, here called secondary nodules, may contribute to the notch effect (see Fig. 1c). Sometimes, secondary nucleation can also imply an accelerated nodule growth rate resulting in extreme warts. The conditions controlling this phenomenon are not clear, but the result is a further increased notch effect. An example of this type of secondary nodule is shown in Fig. 3. It is clearly seen that a crack has started along the common boundary between the secondary nodule and two normal nodules.

3.1.4. Radial cracks

Radial cracks were observed in about 50% of the non-fractured fibres after transverse sectioning and polishing, but rarely in oblique (45°) sections. Further, a great deal of the fracture surface (except "type II") had no detectable radial cracks. Thus the radial cracks are not present along the whole of the filament before the tensile test, which indicates that they are not necessarily a result of residual stresses. It is even possible that they are formed during specimen preparation procedures, such as cutting or polishing.

Sometimes, fracture nucleation could be traced to the outer edge of the radial crack (see Fig. 4), i.e. in the transition region between compressive and dilational residual stresses. (Crack nucleation within the thin region of compression was, as expected, never observed.)

Fig. 4a and b represent a pair of fracture surfaces. The bright contrast (at A) has an intensity profile according to Fig. 5a. In terms of the so-called tip effect, this contrast corresponds to a thickness profile according to Fig. 5b. Because the left–right symmetry is identical across the bright contrast in Fig. 4a and b, the two fracture surfaces, when turned together will fit along a step as shown in Fig. 6a. It is then probable that the step corresponds to a radial shear crack, which has split a transversely propagating fracture front into two different planes as schematically demonstrated in Fig. 6b.

In the region of compressive stress, outside the radial crack edge, the two displaced fracture propagation planes must join. In the correspond-

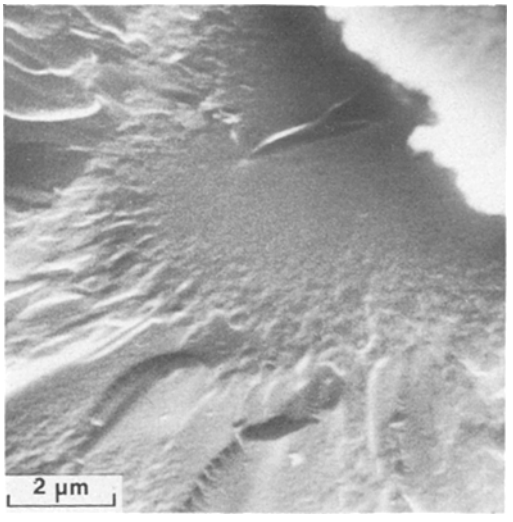

Figure 7 Fracture nucleated at an elongated void on the boron side of the core–mantle interface. The void extends 1 to 3 μm from the interface (fibre B, $\sigma_f = 29.6 \times 10^2\,N\,mm^{-2}$).

ing sloped surface (B in Fig. 4a and b) extremely small steps can be seen. Fig. 4c and d show these steps in high magnification. The image sequence of Fig. 4 provides strong evidence for the nucleation of transverse fracture at the edge of pre-existing radial cracks. This view is further supported by the conventional tracing back of the hackle marks into the mirror zone.

Concerning the radial crack itself, it is also seen from Fig. 4 that it continues through the mantle–core interface, into the core. A detailed view of the interface passage is given by Fig. 10, where the crack apparently coincides with a core surface notch (at A).

3.1.5. Voids near the core–mantle interface

Fig. 7 shows an example of crack nucleation just outside the core–mantle interface. The hackle marks point at an elongated void, which may be the result of vacancy condensation according to the diffusion mechanism discussed by Wawner [8], as mentioned in the Introduction. The diffusion distance x from the void to the core is related to the activation energy E_D for self-diffusion by Einstein's formula

$$x = \sqrt{(2D_0 t)}\exp(-E_D/2kT) \qquad (1)$$

where $D_0 = a^2\nu_0$ is the self-diffusion coefficient (a = shortest interatomic distance, ν_0 = the Debye frequency). Solving E_D as a function of x, with the numerical values $a = 1.76 \times 10^{-4}\,\mu$m

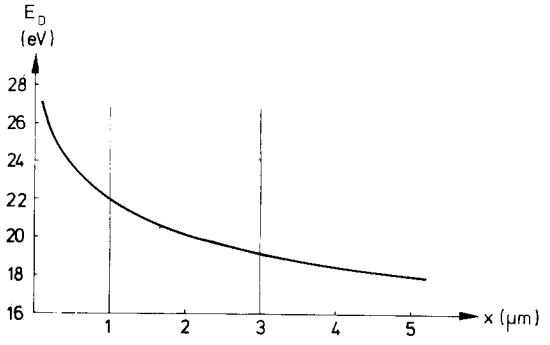

Figure 8 The self-diffusion activation energy E_D, plotted versus the diffusion distance x, according to Equation 2. The measured x interval is introduced in the graph.

$\nu_0 = 10^{13}s^{-1}$, $t = 40$ sec, $T = 1500$ K, gives the activation energy (in eV)

$$E_D = 2.19 - 0.26 \cdot \ln x. \qquad (2)$$

Measurement on the micrographs for the nearest and the most distant void tips provides the x interval (in μm)

$$1 < x < 3 \qquad (3)$$

which corresponds to an activation energy

$$1.9 < E_D < 2.2. \qquad (4)$$

E_D is plotted versus x according to Equation 2 in Fig. 8. Because $\ln x$ is multiplied by a small factor, the present method of estimating E_D is not critically sensitive to uncertainties in x within the considered interval. For much lower x values, however, the curve becomes very steep. During the diffusion process, the core surface has moved outwards. Thus, measuring x directly from the plate, underestimates the diffusion distance somewhat, and the whole interval seems safely outside the steep region.

As far as the authors know, no measurement of the activation energy for self-diffusion in boron has been reported. Considering the strong cohesive forces, as well as the contradictory ease, with which interstitial type self-diffusion can take place in boron, the obtained values seem reasonable. An image of a "proximate void" published by Layden [3], shows the same order of magnitude of the diffusion distances. Thus, there is experimental evidence in favour of the idea of diffusion induced voids outside the core.

3.1.6. Core surface notches

Fracture nucleation at pre-existing core surface notches was observed. The notches may be very

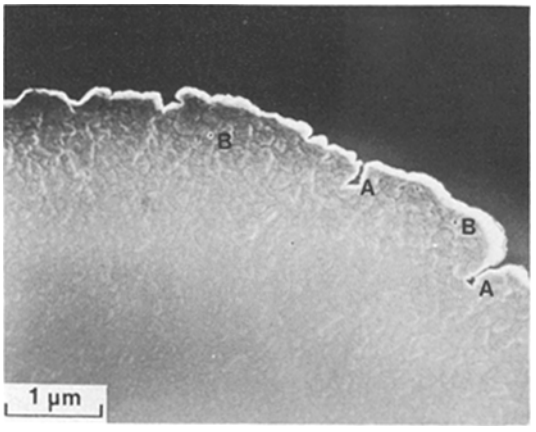

Figure 9 200 kV SEM micrograph showing a transverse section etched by means of an ion beam. The darker region corresponds to the boron mantle (low secondary electron yield). Several notches in different stages of void oclusion can be observed (A). Completely ocluded microvoids are observed at B.

deep and narrow, as shown in high magnification in a polished cross-section in Fig. 9. The formation of voids at the bottom of a notch is particularly well demonstrated at A. As pointed out by Layden [3] the deposition of boron proceeds at a lower rate near the bottom of a deep groove than near the opening, which may result in a gradual hedging-in of a void along the bottom This is well demonstrated at A.

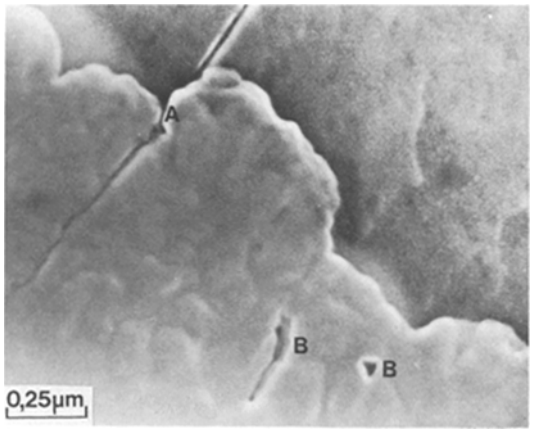

Figure 10 200 kV SEM micrograph of a transverse section of an A_1 fibre. A radial crack cuts through the core at a notch (A). Voids are seen well inside the interface at B.

It is even possible to resolve voids after completed closing of the notch (at B). Similar voids are shown in still higher magnification in Fig. 10.

3.1.7. Core

The mirror zone frequently occurs inside the core

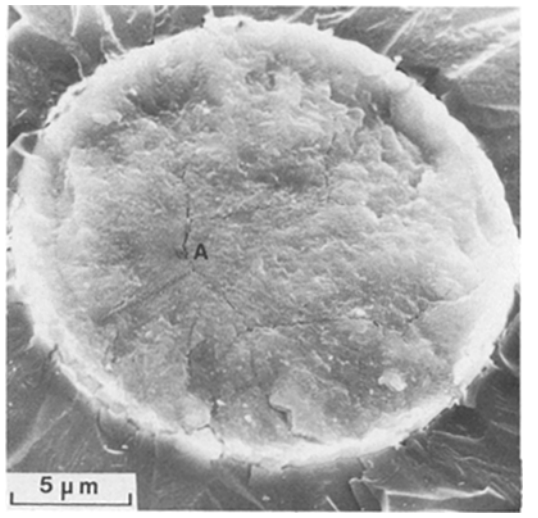

Figure 11 Core initiated fracture (fibre A_1, $\sigma_f = 34.6 \times 10^2\,N\,mm^{-2}$). The mirror zone shows an apparent inclusion at A. Severe cracking of the core and cohesion failure along the interface are observed.

with no particular resolvable initiating flaw, in agreement with earlier observations [3]. In this case the core remains essentially intact. Sometimes, however, an inclusion is found at the center of the mirror zone (Fig. 11). After this type of fracture the core is always plastically deformed and severely cracked. The cohesion along the interface is generally broken.

Also in polished sections of non-fractured surfaces small voids can be observed well within the core, as shown in Fig. 12 (the long crack across the image is a radial crack). Comparison with Fig. 10 shows a striking similarity in the triangular shape of the small voids, indicating the possibility that they are connected to triple nodes between boride grains.

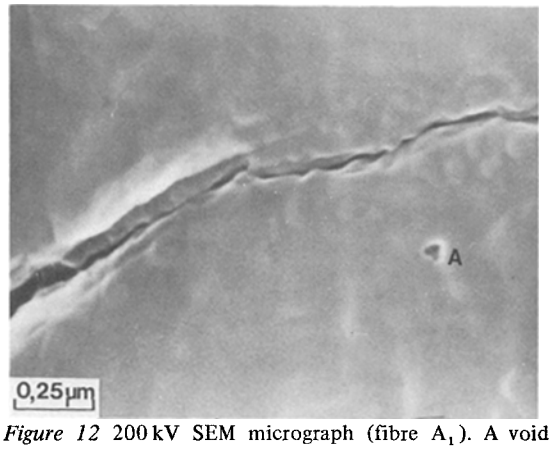

Figure 12 200 kV SEM micrograph (fibre A_1). A void of triangular shape is observed at A, well within the core (compare the similarly shaped void in Fig. 10).

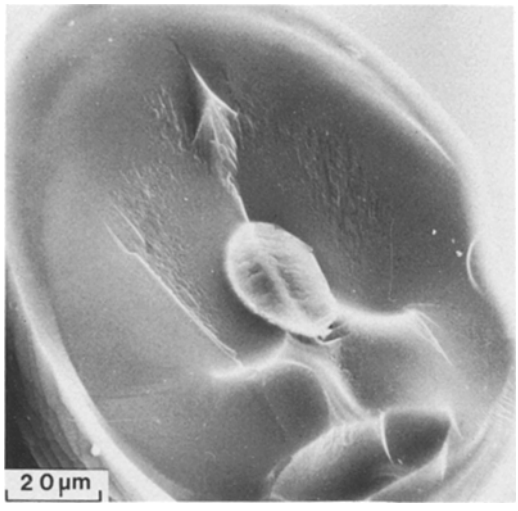

Figure 13 Type II fracture (fibre A_1, $\sigma_f = 35.1 \times 10^2$ N mm^{-2}), initiated in the core.

3.1.8. "Type II" fracture

Fig. 13 shows a "type II" fracture nucleated in the core. A high magnification micrograph of the core shows interior and interface cracking (Fig. 14a). A comparison with the opposite fracture surface (Fig. 14b) shows that the two elevated ridges correspond in position to each other, and thus that considerable plastic deformation was caused by the fracture mechanisms.

3.2. Relation between tensile strength and crack nucleation

All fibres exhibited a linear stress–strain relation to failure. The fracture stress showed the wide scattering typical of most brittle materials. Histograms of the obtained fracture stresses for the three spools are reproduced in Fig. 15. As can be seen, the spools differ significantly in strength.

The crack nucleation mechanisms were grouped and related to fracture stress intervals as indicated in Fig. 15. The lowest fracture stress is related to nucleation at radial cracks (R), and was mainly restricted to spool A_2. Surface nucleation (S) at nodule boundaries, corresponding to badly oriented growth and secondary nodules are less severe, while nucleation in the core–mantle region (CM) and within the core (C), respectively, are related to successively higher strengths.

Obviously, fibre A_1, which suffers mainly from core and interface crack nucleation, exhibits a better nodular growth, with larger notch angles than the others. Above all it is completely free from radial cracks. This indicates that radial cracks observed in fracture surfaces should not have been created by the fracture. An exception is the "type II" fracture, in which a radial crack is obtained during the tensile test, and propagates together with two similar cracks (the "gull wings") from a nucleation site within the core [3]. Consequently, this type of fracture does not correspond to the low strength typical of the R region in Fig. 15, but rather to the strong C region as demonstrated both by the present results and Layden's results.

A further comment is that the fibre investi-

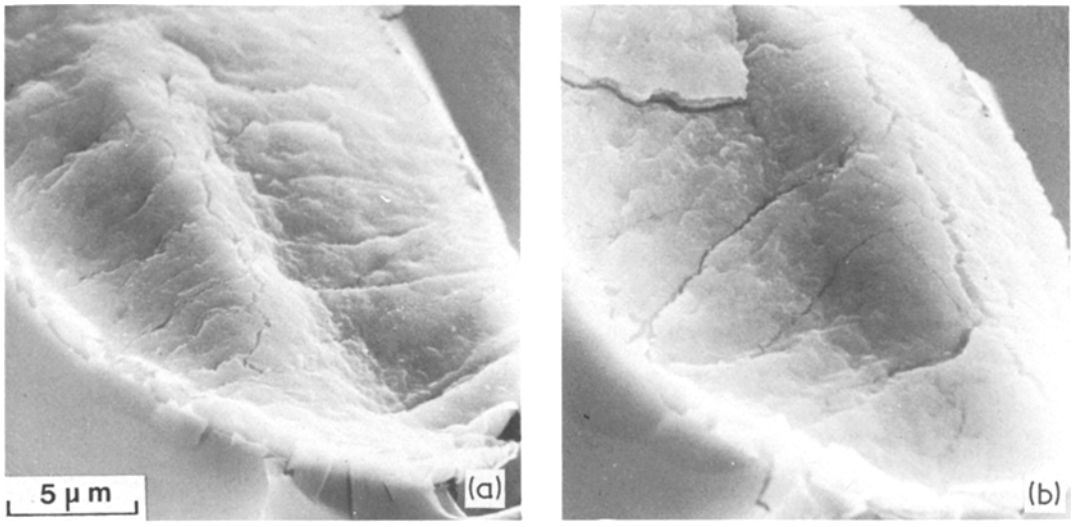

Figure 14 The core regions of the two fracture surfaces corresponding to Fig. 3. The bright ridges correspond in position to each other.

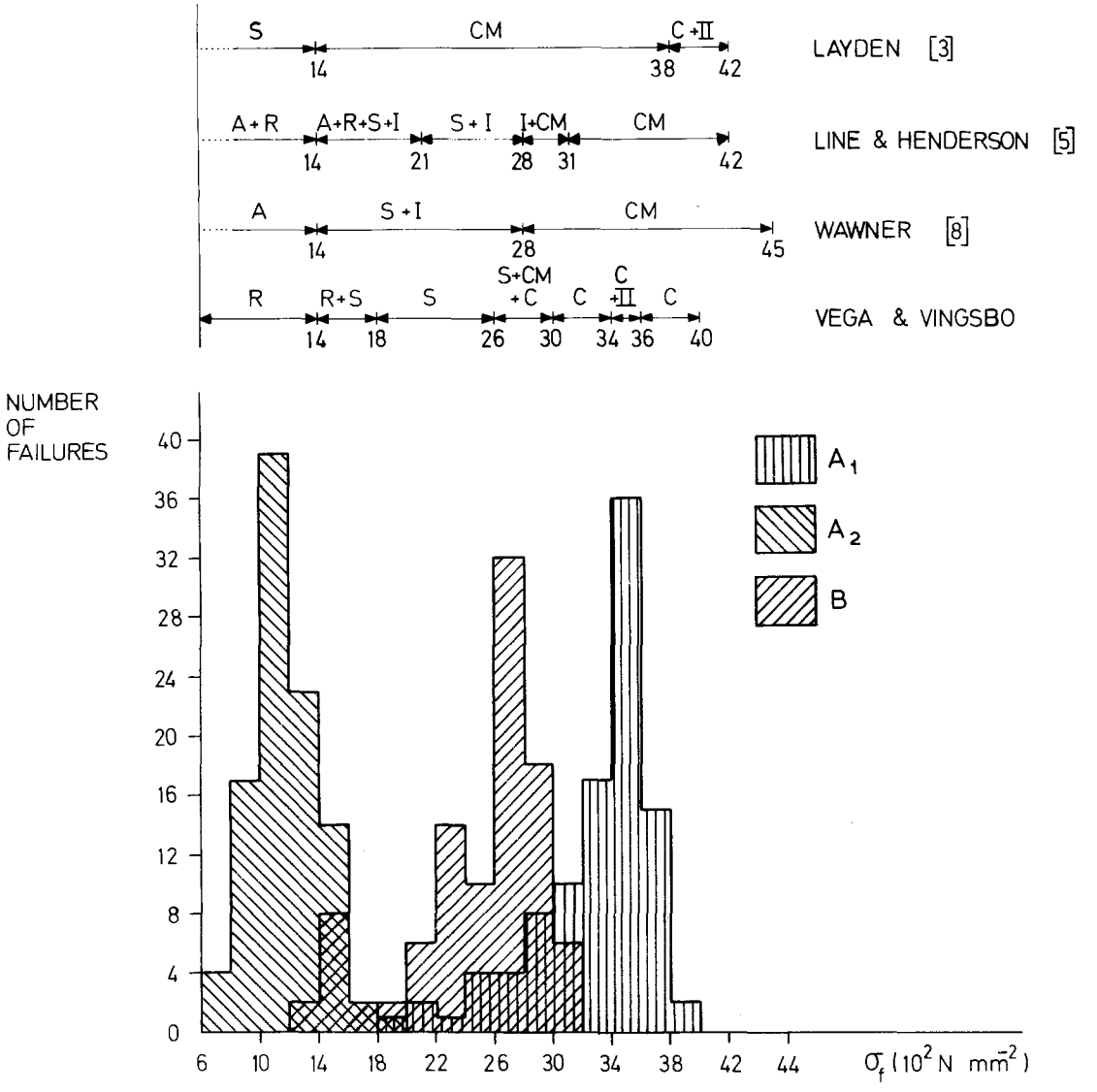

Figure 15 Histograms of the fracture stresses for spools A_1, A_2 and B, corresponding to 100 tests for each spool. Above the histograms, the crack nucleation mechanisms have been grouped, related to fracture stress intervals and compared to results of earlier investigations. The following abbreviations are used: A: abnormal crystalline growth R: radial crack, S: surface flaws, i.e. abnormal and secondary nodular growth, I: inclusions, CM: flaws at, or in the vicinity of, the core–mantle interface, II: type II [3], C: core.

gated by Layden was similar to our A_1 fibre, and of a high quality. The fibres investigated by Wawner and by Line and Henderson were manufactured in a less clean process which gave inclusion induced fracture. In addition, a critically high reaction temperature may have resulted in crystalline mantle growth.

4. Summary and conclusions

It has been shown with good statistical significance that continuous boron fibres have well-defined fracture properties, typical of the individual fibre. Tensile strength histograms reveal that the individual properties are clearly distinguishable from one fibre, i.e. one set of manufacturing parameters, to another.

Although the σ_f distribution tails may be long, the half-widths are always narrow. Therefore, comparison of different strength intervals only, will not provide the total information on fibre typical properties, which can be revealed by the complete strength distribution curves.

Further, there is a strong correlation between the tensile strength and the type of transverse

crack nucleation. The crack nucleation, in its turn, is related to structural imperfections, some of which can be controlled by the fibre manufacturing conditions.

The most critical weakening imperfection seems to be radial cracks. It has not yet been possible to find the cause of these cracks. The present investigation gives some evidence that they are neither fracture induced, nor an exclusive result of residual stresses. This favours the idea that the radial cracks should be formed during specimen preparation (cutting, grinding etc) for subsequent studies (mechanical testing, microscopy etc.), but does not exclude the possibility of quench stress induced cracking, e.g. in combination with rolling on spools.

Important quality parameters, which can be controlled, are the purity of the reacting gases and the nodular growth.

Acknowledgements

The authors are grateful to Fil.Lic. Tommy Lindahl, Fil.Mag. Jan Otto Carlsson, Docent Axel Rönnquist and Docent Torsten Lundström for invaluable advice and help during the whole of this work. Thanks are also due to Mr Rein Kalm for skilful technical assistance and to Miss Ingrid Strandh for instructive and beautiful drawings. The tensile testing was performed at Lumalampan AB, Stockholm.

References

1. C. P. TALLEY, L. LINE and Q. OVERMAN in "Boron Synthesis, Structure and Properties" edited by I. Kohn, W. Nye and G. Gaulé (Plenum Press, New York, 1960).
2. E. H. ANDREWS, *J. Appl. Phys.* **30** (1959) 740.
3. G. K. LAYDEN, *J. Mater. Sci.* 8 (1973) 1581.
4. F. WAWNER JUN., in "Boron", Vol. II, edited by G. Gaulé (Plenum Press, New York, 1965).
5. L. E. LINE JUN. and U. V. HENDERSON JUN., in "Handbook of Fiberglass and Advanced Plastic Composites", edited by G. Lubin, (Van Nostrand Reinhold, New York, 1969).
6. F. E. WAWNER and D. SATTERFIELD, *Appl. Phys. Letters* **11** (1967) 192.
7. A. MACHONIS, *Grumman Research Department Report, RE 270 (October 1966).*
8. F. E. WAWNER JUN., in "Modern Composite Materials", edited by L. J. Broutman and R.H. Krock (Addison Wesley, 1967).
9. J. O. CARLSSON, Department of Inorganic Chemistry, Uppsala University, Uppsala, Sweden, private communication.

Received 25 June and accepted 29 July 1975.